



JOINT INSTITUTE FOR NUCLEAR RESEARCH  
Veksler and Baldin Laboratory of High Energy Physics

# FINAL REPORT ON THE SUMMER STUDENT PROGRAM

Study of charged particle production and  
particle ratios at MPD experiment with  
Monte-Carlo simulations

**Supervisor:** Alexey Aparin, JINR  
**Student:** Elena Andreevna Pervyshina, Russia  
Lomonosov Moscow State University  
**Participation Period:** July 07 - August 24

Dubna, 2019

## Abstract

In this report an analysis of inclusive particles in collisions of  $Au - Au$  ions with the collision energies  $\sqrt{s} = 4, 7, 9, 11$  GeV. The spectra of particles depending on the transverse momentum for the identified hadrons (kaons, pions, protons) were obtained, and the strangeness production behavior in collisions of heavy ions was analyzed by calculating the ratio  $K^+/\pi^+$ . Statistics were collected using Monte Carlo generator Ultra-relativistic Quantum Molecular Dynamic (UrQMD) for Multi Purpose Detector (MPD) geometry made in Geant 4 model. Our goal was to investigate one of the signatures of the phase transition between the hadron state of matter and the of quark-gluon plasma (QGP) state. We also present a brief introduction to quantum Chromodynamics and phase diagram of nuclear matter.

## Contents

<b>1</b>	<b>Introduction</b>	<b>3</b>
<b>2</b>	<b>NICA Experiment</b>	<b>4</b>
2.1	Multi Purpose Detector . . . . .	5
<b>3</b>	<b>UrQMD Model</b>	<b>6</b>
<b>4</b>	<b>Analysis of results</b>	<b>6</b>
4.1	$p_T$ spectra for different particles . . . . .	7
4.2	$K^+/\pi^+$ and $K^-/\pi^-$ ratios . . . . .	12
4.3	$K^-/K^+$ , $\pi^-/\pi^+$ and $p^-/p^+$ ratios . . . . .	13
<b>5</b>	<b>Conclusion</b>	<b>17</b>
<b>6</b>	<b>Acknowledgements</b>	<b>17</b>

# 1 Introduction

Experiments on heavy-ion collisions at high energies provided a unique opportunity to study nuclear matter at extreme barionic densities and temperatures. Different theoretical models are used to describe such collisions, involving different interaction scenarios, so that new experimental data with high resolution and large statistics are needed to verify different theoretical predictions. Quantum chromodynamics (QCD) is used as the basis theory of strong interactions. But unlike the Quantum Electrodynamics, exact theoretical calculations of the QCD lagrangian is not possible due to the effect of color anti-screening.

Quantum chromodynamics is a theory of strong interactions in which the fundamental objects are quarks, antiquarks, and gluons that are not observed in the free state. In the quark model, hadrons consist of fundamental components quarks or antiquark and gluons. The quark model in its naive form is not complete, since not all hadrons follow the Pauli principle. To solve this problem, the presence of an additional quantum number, color, was postulated. Quarks can exist in three different color states, called red, green, blue. Within QCD, matter can exist in various phase states, in addition to the usual nuclear matter.

QCD matter can be described in terms of thermodynamical potentials. On Figure 1 a scheme of the phase diagram of nuclear matter is plotted.

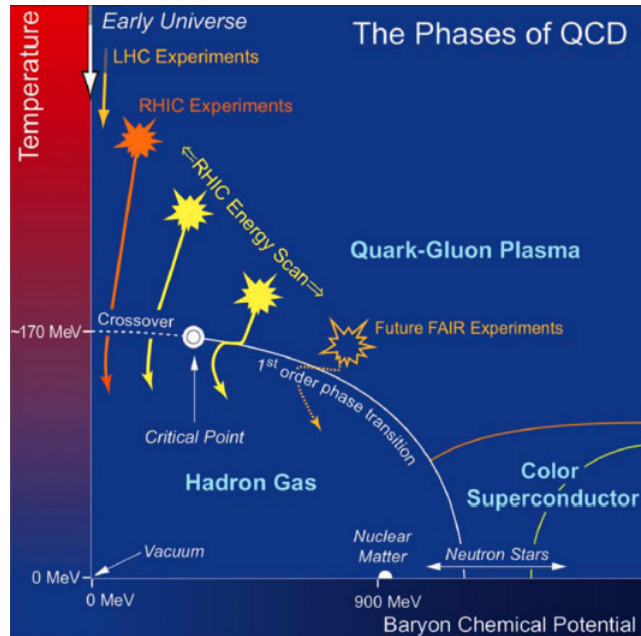


Figure 1: A conjectured QCD phase diagram of nuclear matter with  $\mu_B$  on the horizontal axis and Temperature (in energy units) on vertical axis. Figure taken from [2]. Different points correspond to different experimental conditions. Solid lines are schematic boundaries of different phases predicted from theoretical models.

The most accessible way of experimentally characterizing the phase diagram is in the plane of temperature ( $T$ ) and baryon chemical potential ( $\mu_B$ ), as shown in Figure 1. For values close to  $\mu_B = 0$ , experiments at the Large Hadron Collider (LHC) and the Relativistic Heavy Ion Collider (RHIC) have provided evidence of the QGP formation, but exact parameters of the first order phase transition location and existence of the critical point at higher  $\mu_B$  is yet to be confirmed experimentally.

In this work, the particle production ratios for different types of charged hadrons  $\pi^+/\pi^-$ ,  $K^+/K^-$ ,  $K/\pi$  were investigated in collisions of  $Au - Au$  ions as the signature of the phase transition. The increase in strangeness production was predicted as a signature of the formation of QGP [1]. The formation of quark-gluon plasma is not expected to occur at low collision energies, so the increased formation of oddities in collisions of heavy ions compared to  $p - p$  can be a sign of the formation of QGP. Although this is

not a sufficient signature, the presence of enhanced weirdness production is a necessary condition for the formation of QGP.

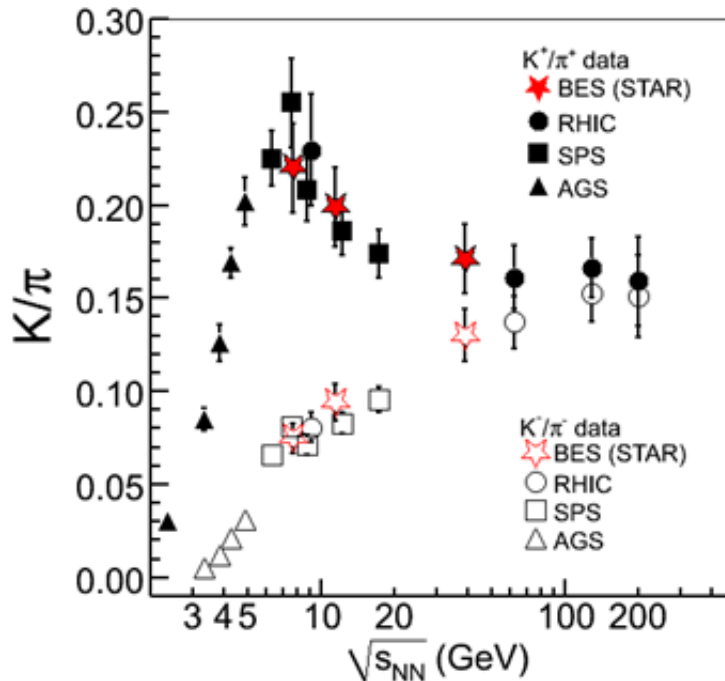


Figure 2: Experimental data from the  $K/\pi$  ratio in central heavy ion collisions and in  $p-p$  collisions. It shows a peak in the  $K^+/\pi^+$  production, referred to as "the horn".

Figure 2 shows the energy dependence of  $K/\pi$  particle ratio. The  $K/\pi$  ratio is of interest, as it reflects the strangeness content in heavy-ion collisions. An enhancement in  $K/\pi$  ratio in heavy-ion collisions compared to  $p-p$  collisions has been taken previously as an indication of QGP formation [3]. The peak position (horn) in energy dependence of  $K^+/\pi^+$  has been suggested as the signature of a phase transition from hadron gas to a QGP while going from lower to higher energies. However, various models that do not include such a phase transition claim to explain this type of energy dependence of the  $K^+/\pi^+$  ratio. It may be noted that the peak position around 7.7 GeV corresponds to an energy where the maximum baryon density is predicted in heavy-ion collisions.

## 2 NICA Experiment

NICA (Nuclotron-based Ion Collider Facility) is a new accelerator complex which is now constructed at the Joint Institute for Nuclear Research (Dubna, Russia) to study properties of dense baryonic matter. After putting the NICA collider into operation JINR will be able to create in the Laboratory of high energy physics a special state of matter in which our Universe stayed shortly after the Big Bang the Quark-Gluon Plasma.

Specific scope elements of the project facility should include: Injection complex, new superconducting Booster synchrotron (that will be located inside the yoke of the decommissioned Synchrophasotron), the existing superconducting heavy ion synchrotron Nuclotron, collider having two new superconducting storage rings, new beam transfer channels. The location of all components is shown in the Figure 3.

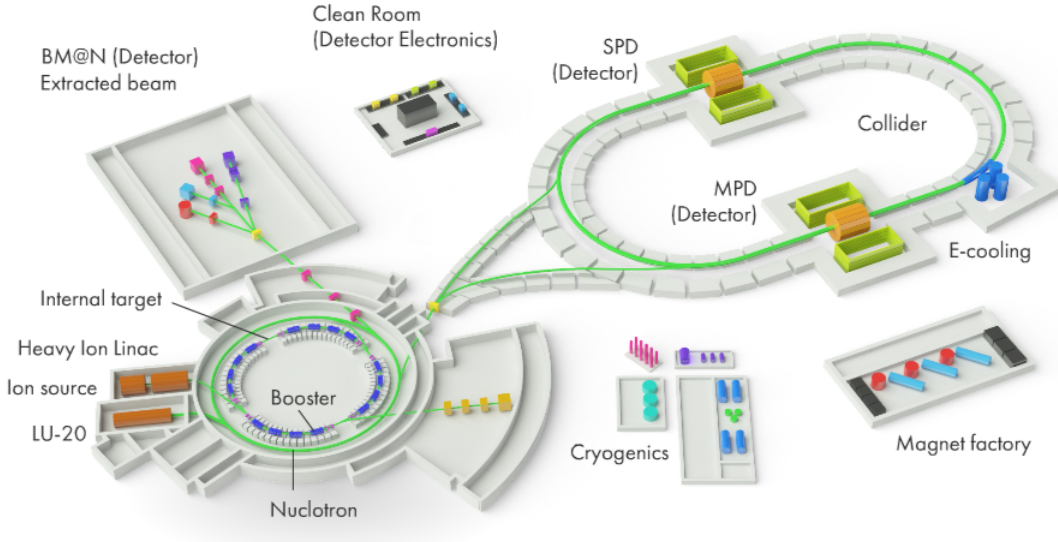


Figure 3: Scheme of the future NICA Complex [4].

The possible creation of a quark-gluon plasma in ultra-high-energy nuclear collisions has been (and still is) extensively studied at RHIC and LHC and there is strong circumstantial evidence that such a phase is indeed created in those reactions. As the collision energy decreasing from the top RHIC energy (200 GeV per nucleon-nucleon pair) to the lowest SPS energy (5 GeV per nucleon-nucleon pair), the maximum energy density created also decreases and, consequently, there is a certain transition region of collision energy below which it is no longer possible to access the plasma phase in the course of the collision. The energy range of NICA is sufficiently large to encompass both collisions in which the plasma phase is well developed and collisions in which the matter remains purely hadronic throughout. Thus NICA is ideally suited for exploring the transition between the familiar hadronic phase and the new plasma phase. [5]

In order to achieve the projected luminosity at required energies additionally to the existing Nuclotron accelerator of heavy ions the project foresees the construction of a booster ring and new ion source for the NICA complex. There would be two experimental detectors to study heavy ion collisions in collider mode - a Multi-Purpose Detector (MPD), and a Baryonic Matter at Nuclotron (BM@N) experiment for fix-target experiment.

## 2.1 Multi Purpose Detector

The MPD detector has been designed as a 4 spectrometer capable of detecting charged hadrons, electrons and photons produced in heavy-ion collisions at high luminosity in the energy range of the NICA collider  $\sqrt{s_{NN}} = 2 - 12$  GeV for  $Au - Au$  collisions. To reach this goal, the detector should comprise a precise 3-D tracking system and a high-performance particle identification (PID) system based on the  $dE/dx$  technique in Time Projection Chamber (TPC) and  $1/\beta$  time-of-flight measurements. The general layout of the MPD apparatus is shown on Figure 4. The whole detector setup includes Central Detector (CD) covering  $\pm 2$  units in pseudorapidity ( $\eta$ ). [4]

The processes investigated in this work were studied with MPD Monte-Carlo simulations using the dedicated software framework (MpdRoot). This software is based on the object-oriented framework FairRoot and provides a powerful tool for detector performance studies, development of algorithms for reconstruction and physics analysis of the data.

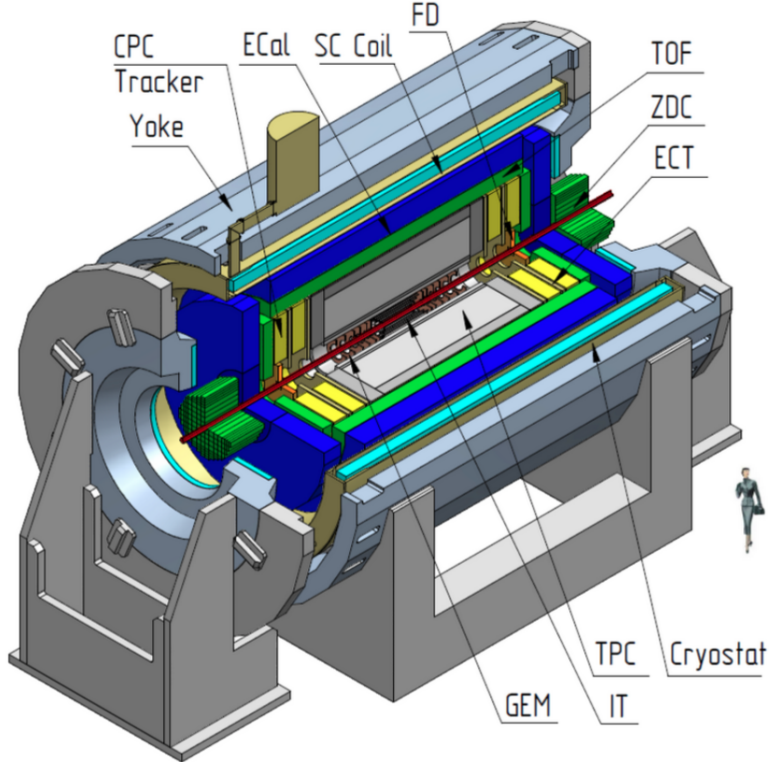


Figure 4: Planned scheme of NICA Multi Purpose Detector layout [6].

The MPD detector consist of three major parts: Central Barrel detector, and (FS-A, FS-B) - two forward spectrometers (optional). The following subsystems are drawn on figure 4: superconductor solenoid (SC Coil) and magnet yoke, inner detector (IT), straw-tube tracker (ECT), time-projection chamber (TPC), time-of-flight system (TOF), electromagnetic calorimeter (EMC), fast forward detectors (FFD), and zero degree calorimeter (ZDC).

### 3 UrQMD Model

Ultra-relativistic Quantum Molecular Dynamic (UrQMD) - is a microscopic Monte-Carlo model based on the use of phase space to describe nuclear reactions. It describes the hadron interaction at low energies ( $\sqrt{s} < 5$  GeV) as the interaction between hadrons and resonances. The model describes the hadron interaction at high energies ( $\sqrt{s_{NN}} > 5$  GeV) as excitation of colored strings with their subsequent fragmentation into hadrons. It should be noted that there is no single theoretical description that would fully explain the mechanism of hadron-hadron interaction for different collision energies and different kinematic conditions.

The model is based on the covariant propagation of all hadrons considered at the quasi-particle level in classical trajectories combined with stochastic binary scattering, colored string formation, and resonance decay. This model is used as a simulation package for proton-proton, proton-nucleus and nucleus-nucleus interactions. To run this program, the energy in the center-of-mass frame ( $\sqrt{s_{NN}}$ ), the number of events and the freeze-out time were given as the input for  $Au - Au$  collisions.

It is important to say that UrQMD model doesn't have a phase transition mechanism, this should be taken into account when comparing the results to the respective experimental ones.

### 4 Analysis of results

The nucleus-nucleus collision is considered as a process of interactions between single nucleons. The dynamics of these collisions can be explained using the space-time diagram in figure 5. Consider the frontal

collision of two nuclei moving along the beam direction. After the collision, nucleons inside the overlap area begin to interact, creating a substance with density much higher than the normal density of nuclear matter. The values of energy density and temperature can increase to the critical values, reaching a sufficient value to overcome the confinement of quarks and gluons, of which hadrons are composed, and a quark-gluon plasma can be formed. Over time, quasi-equilibrium is achieved, and free quarks and gluons form hadrons again. If this phase transition from quarks and gluons to hadrons is of the first order, it will pass into the mixed phase at some critical temperature. It is assumed that the temperature of the system will remain constant in the mixed phase like in any other thermodynamical system. The transition from quarks and gluons back to hadrons will mean the end of the mixed phase. System continue to cool and expand consisting of hadron gas. As a result of the termination of inelastic interactions, the processes of particle production stops, this means that the system has reached chemical equilibrium. This time (or temperature) at which inelastic interactions stop is called the time (or temperature) of chemical freezing. After that, the system continues to cool down and expand, but only with elastic interactions. When the time (temperature) is reached, when the distance between any two particles in the medium is greater than the average free path, the elastic collisions stop. It is common to call this time (temperature) the time of kinetic freezing. Particles in this phase leave the system and are detected by the sub-systems of the experiment. Therefore, we can judge the reaction only by the initial and final (products after freezing) states of the participants.

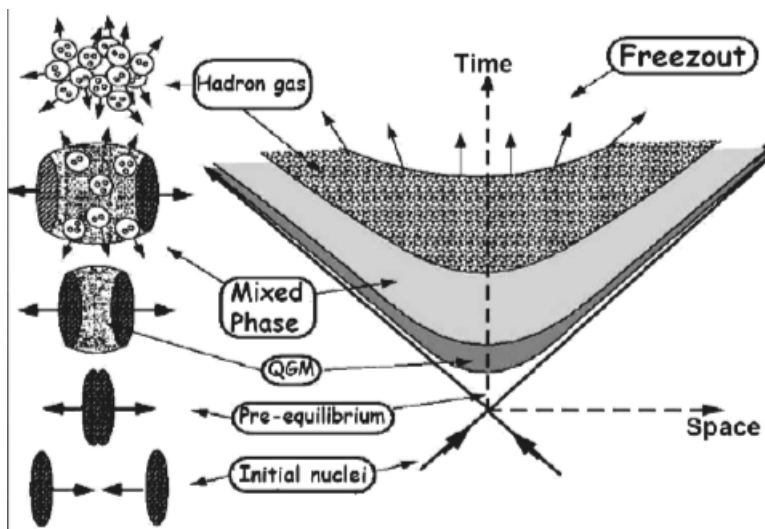


Figure 5: Space-time diagram and various evolutionary stages of the relativistic collision of heavy ions.

#### 4.1 $p_T$ spectra for different particles

Monte-Carlo events were generated for different entrance-of-mass energy of the collision  $\sqrt{s_{NN}} = 4, 7, 9, 11$  GeV. Data for different collision energies allowed to calculate the energy dependence of the particle production in the region where the "horn" effect was observed. The data were obtained from collisions of gold ions  $Au - Au$  using Monte Carlo generator Ultra-relativistic Quantum Molecular Dynamic (UrQMD).

The distributions of the identified particle production on the transverse momentum allow us to judge the kinematics of the process, and also to determine the position of the point on the phase diagram. To do this, we investigate the dependence of the invariant inclusive cross section on the transverse momentum  $\frac{1}{N} \frac{1}{2\pi p_T} \frac{d^2 N}{dp_T d\eta}$ . They were obtained in two intervals of pseudorapidity region  $|\eta| < 0.1, 0.5$ . These spectra were received and calculated using HybriLIT cluster and GOVORUN supercomputer.

The spectra for the transverse momentum  $p_T$  for identified particles are shown in Figure ??, 8 with the cut on the pseudorapidity  $|\eta| < 0.5$  for Figure 10, 11 spectra are presented for transverse momentum  $p_T$  with the cut on the pseudorapidity region  $|\eta| < 0.1$ . For the pseudorapidity region  $|\eta| < 0.1$  spectra are presented, only for pions, to illustrate that the dependencies are not essentially different. Figures 6 and

9 represent the fitted histograms of the transverse momentum. After applying experimental acceptance of the MPD detector, it was decided to use the following transverse momentum range:  $0.2 \leq p_T \leq 1.4$  GeV/c. The results are shown separately for  $\pi^+$ ,  $\pi^-$ ,  $K^+$ ,  $K^-$ ,  $p^+$  and  $p^-$ . The last two bins on the histograms were made wider than the previous ones due to poor statistics for large values of the transverse momentum.

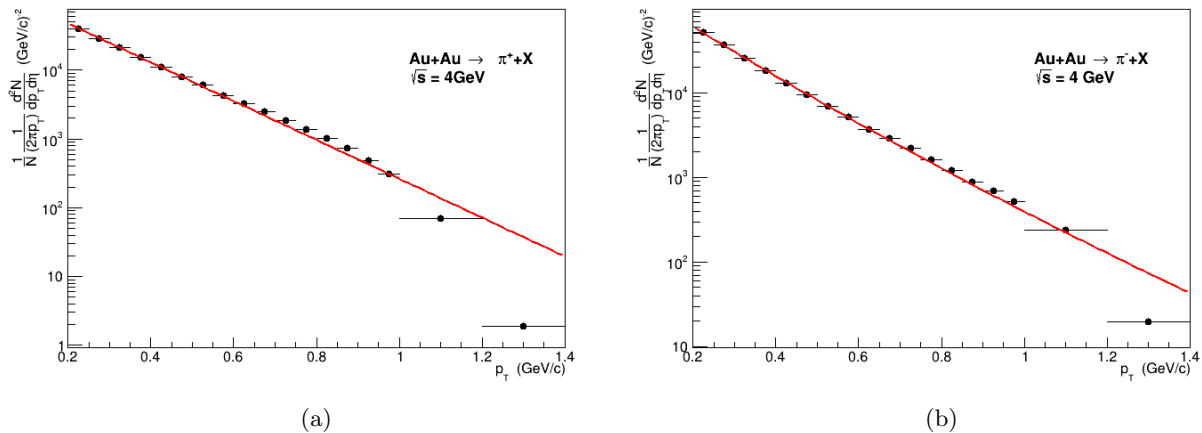
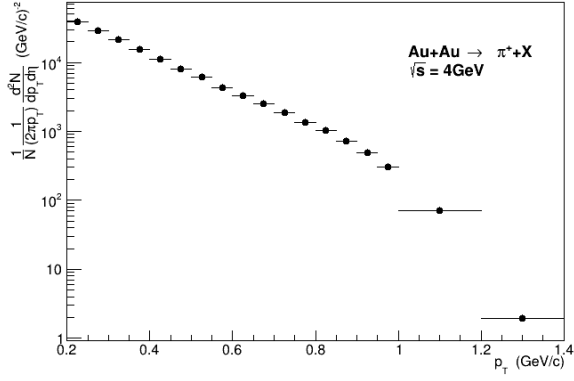
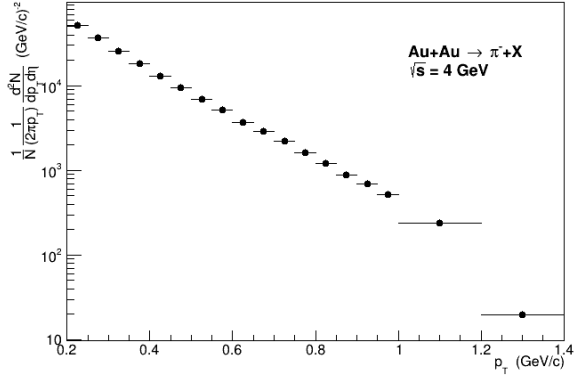


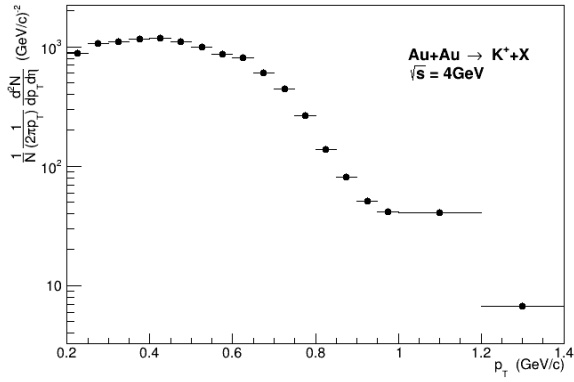
Figure 6: Fitted histograms of transverse momentum for the collision energy  $\sqrt{s_{NN}} = 7$  GeV with pseudorapidity cut  $|\eta| < 0.5$  and  $0.2 < p_T < 1.4$  for different particles: (a)  $\pi^+$ , (b)  $\pi^-$ .



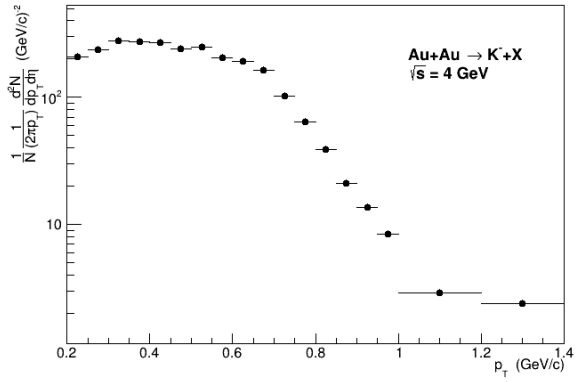
(a)



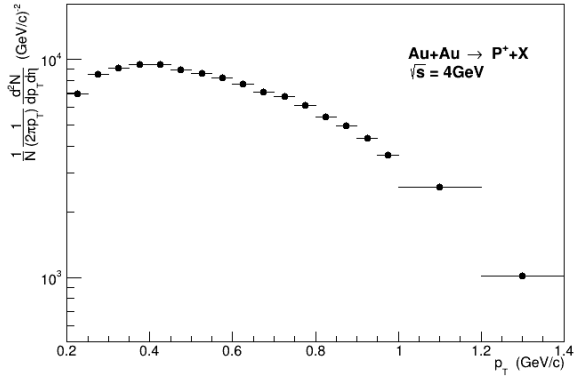
(b)



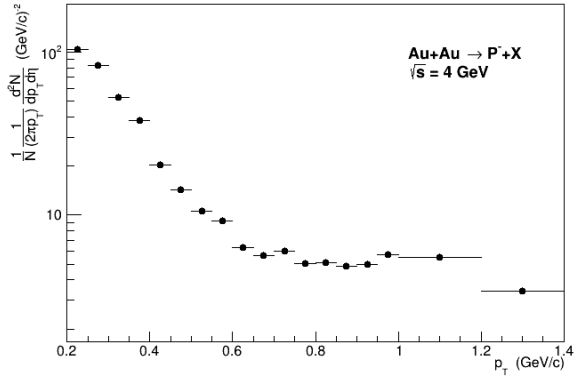
(c)



(d)

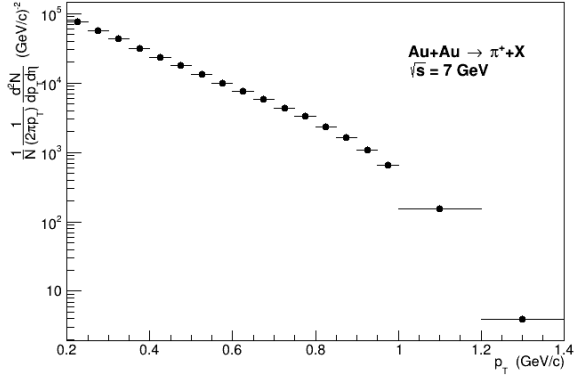


(e)

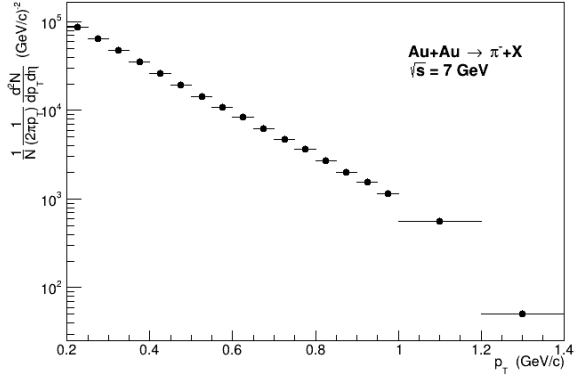


(f)

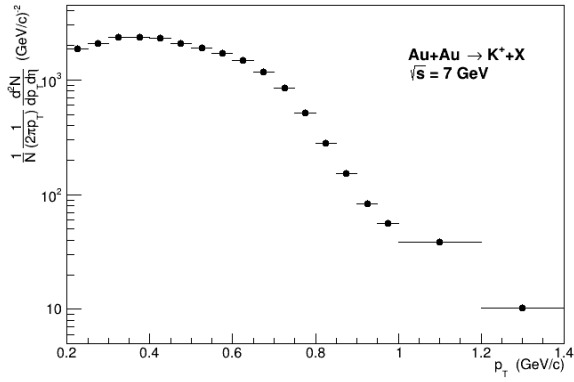
Figure 7: Histograms of transverse momentum for the collision energy  $\sqrt{s_{NN}} = 4$  GeV with pseudorapidity cut  $|\eta| < 0.5$  and  $0.2 < p_T < 1.4$  for different particles: (a)  $\pi^+$ , (b)  $\pi^-$ , (c)  $K^+$ , (d)  $K^-$ , (e)  $p^+$ , (f)  $p^-$ .



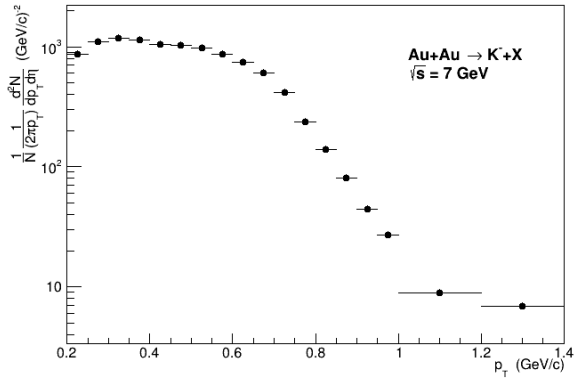
(a)



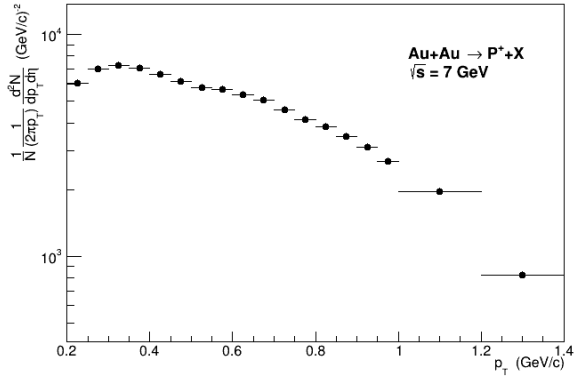
(b)



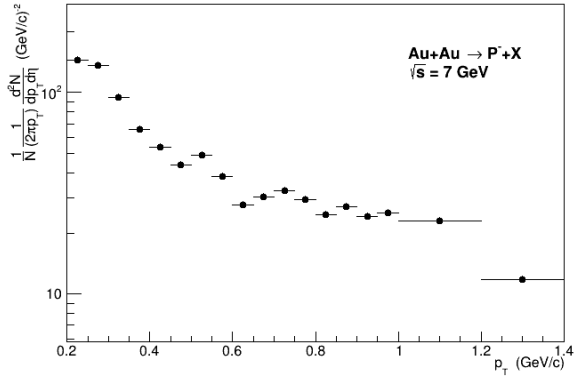
(c)



(d)



(e)



(f)

Figure 8: Histograms of transverse momentum for the collision energy  $\sqrt{s_{NN}} = 7$  GeV with pseudorapidity cut  $|\eta| < 0.5$  and  $0.2 < p_T < 1.4$  for different particles: (a)  $\pi^+$ , (b)  $\pi^-$ , (c)  $K^+$ , (d)  $K^-$ , (e)  $p^+$ , (f)  $p^-$ .

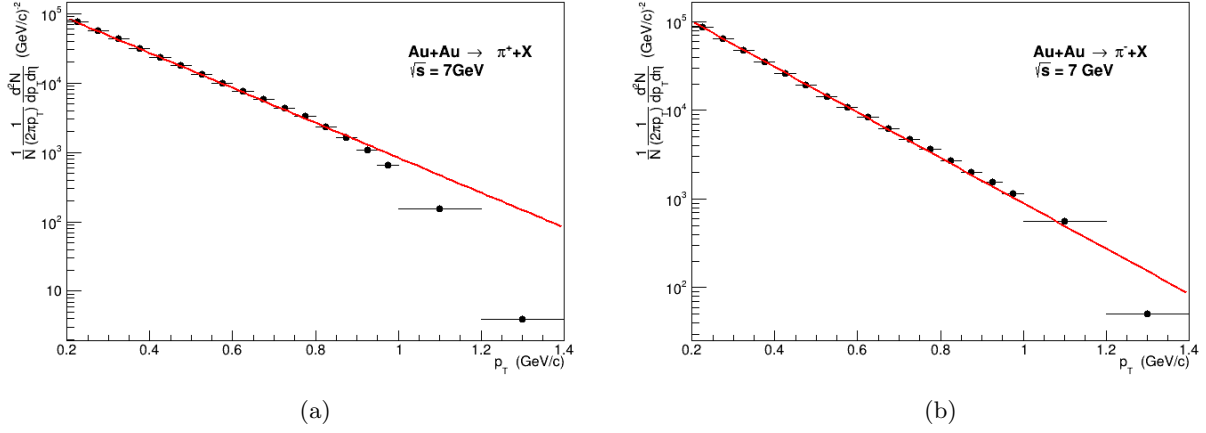


Figure 9: Fits histograms of transverse momentum for the collision energy  $\sqrt{s_{NN}} = 7$  GeV with pseudorapidity cut  $|\eta| < 0.5$  and  $0.2 < p_T < 1.4$  for different particles: (a)  $\pi^+$ , (b)  $\pi^-$ .

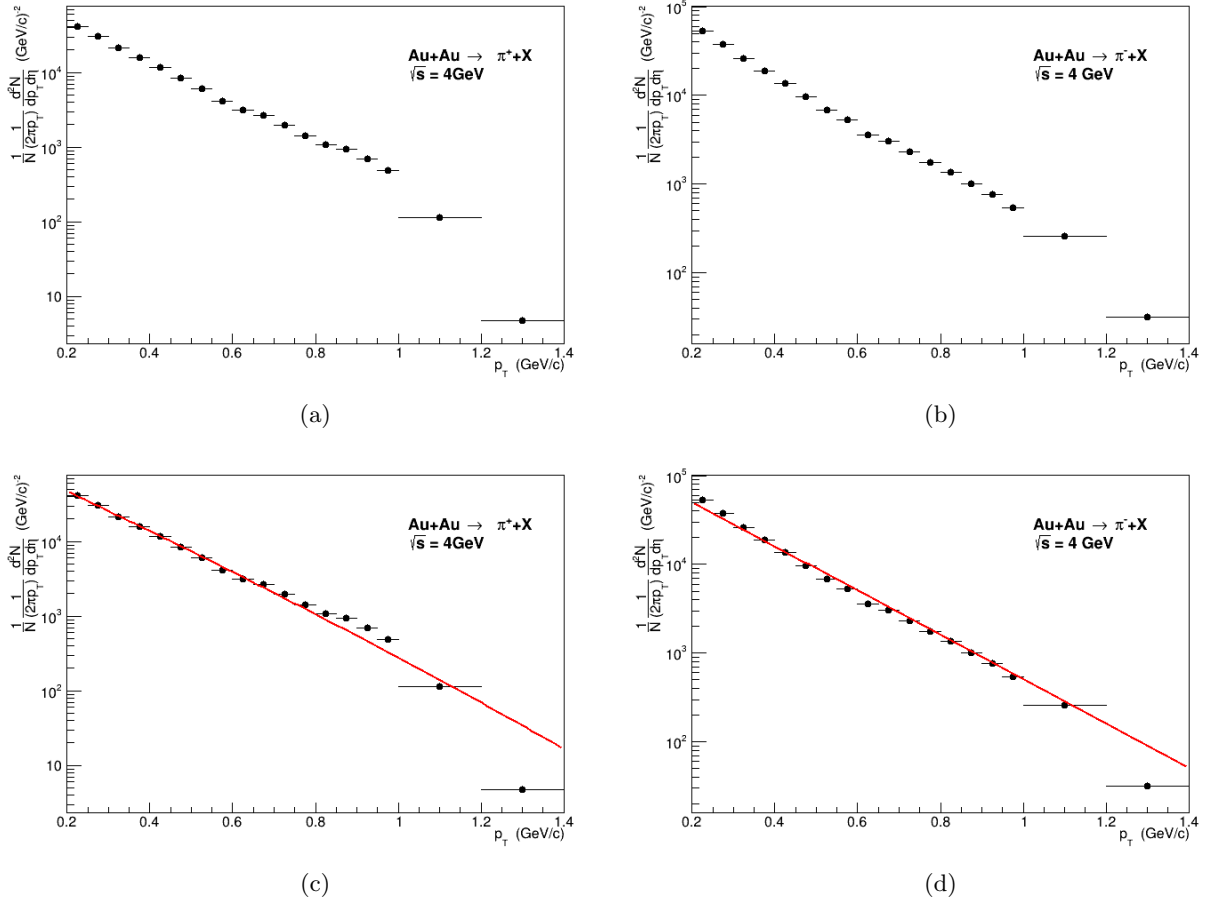


Figure 10: Histograms of transverse momentum and their fits for the collision energy  $\sqrt{s_{NN}} = 4$  GeV with pseudorapidity cut  $|\eta| < 0.1$  and  $0.2 < p_T < 1.4$  for different particles: (a), (c)  $\pi^+$ ; (b), (d)  $\pi^-$ .

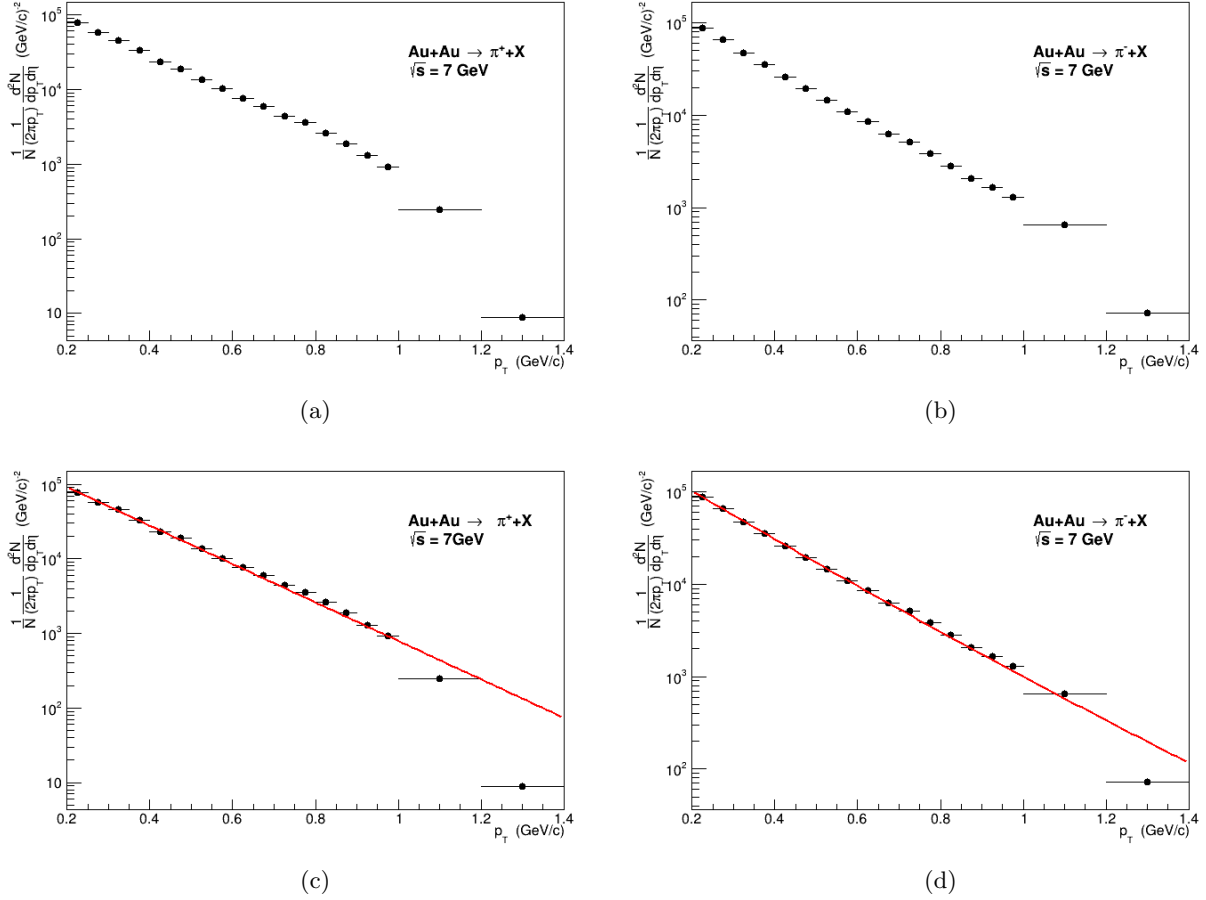


Figure 11: Histograms of transverse momentum and their fits for the collision energy  $\sqrt{s_{NN}} = 7$  GeV with pseudorapidity cut  $|\eta| < 0.1$  and  $0.2 < p_T < 1.4$  for different particles: (a), (c)  $\pi^+$ ; (b), (d)  $\pi^-$ .

## 4.2 $K^+/\pi^+$ and $K^-/\pi^-$ ratios

The  $K/\pi$  ratio is of interest because it reflects the strangeness production in the produced medium in heavy ion collisions. An increase in the ratio of  $K/\pi$  in heavy ion compared to  $p-p$  collisions was previously indicated as a sign of QGP formation [7]. The relations  $K^+/\pi^+$  and  $K^-/\pi^-$  were constructed to test the "horn" effect.

Figures 12, 13 show the energy dependence of  $K^+/\pi^+$  and  $K^-/\pi^-$  particles ratio, the data dependencies are also presented. The data were fitted by the polynomial function  $f(x) = p_0 + p_1 * x + p_2 * x^2 + \dots$ . For  $|\eta| < 0.5$  we used a second order polynomial on  $K^+/\pi^+$  and a third order on  $K^-/\pi^-$ , the same polynomial orders we used for  $|\eta| < 0.1$ . There is a visible increase in the ratio of negatively charged particles ( $K^-/\pi^-$ ) with energy increase, thus for the positively charged particles ( $K^+/\pi^+$ ), on the contrary, there is a decrease. A similar relation is observed for both  $\eta$  intervals.

Figure ?? shows the expected experimental dependence. It is seen that at low energies there should be a continuous increase in the ratio  $K^-/\pi^-$  and a sharp increase to a maximal value in  $K^+/\pi^+$  followed by a decrease ("horn"). This result is not observed in the MC data obtained, which is to be expected since the UrQMD model does not include phase transition as mentioned above.

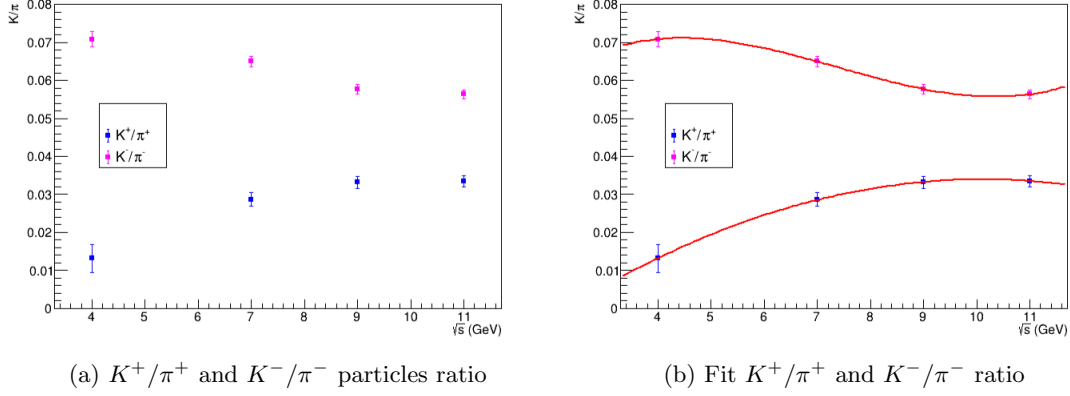


Figure 12: The ratio  $K/\pi$  for the four calculated energies  $\sqrt{s_{NN}} = 4, 7, 9, 11$  GeV with pseudorapidity cut  $|\eta| < 0.5$  and  $0.2 < p_T < 1.4$ . The parameters of the fit for  $K^+/\pi^+$ :  $\chi^2 = 0.00827892$ ,  $p_0 = -0.023 \pm 0.013$ ,  $p_1 = 0.011 \pm 0.003$ ,  $p_2 = -0.00055 \pm 0.00019$ . The parameters of fit for  $K^-/\pi^-$ :  $\chi^2 = 1.01143e - 21$ ,  $p_0 = 0.04 \pm 0.03$ ,  $p_1 = 0.021 \pm 0.015$ ,  $p_2 = -0.003 \pm 0.002$ ,  $p_3 = 0.00015 \pm 0.00009$ .

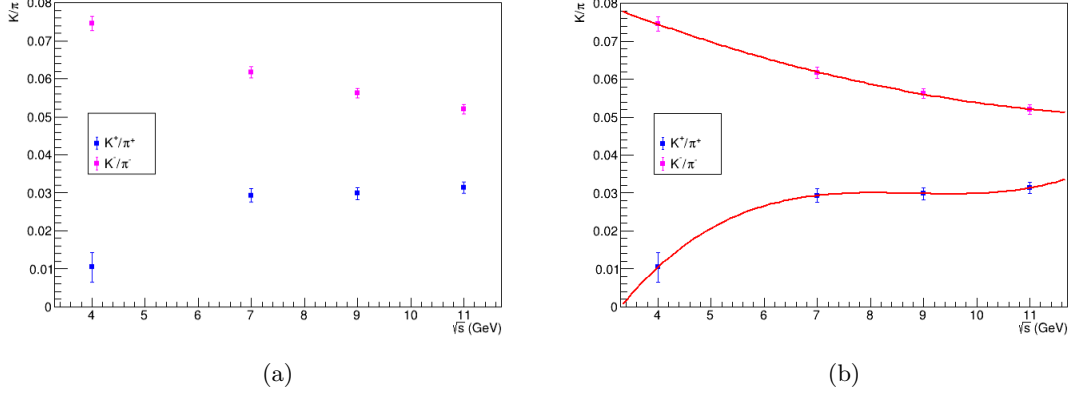


Figure 13: The ratio  $K/\pi$  for the four energies  $\sqrt{s_{NN}} = 4, 7, 9, 11$  GeV with cut of pseudorapidity  $|\eta| < 0.1$  and  $0.2 < p_T < 1.4$  (a) and fits by polynomial function (b). The parameters of fit  $K^+/\pi^+$ :  $\chi^2 = 0.0742329$ ,  $p_0 = 0.098 \pm 0.007$ ,  $p_1 = -0.007 \pm 0.002$ ,  $p_2 = 0.00025 \pm 0.00013$ . The parameters of fit  $K^-/\pi^-$ :  $\chi^2 = 2.51757e - 22$ ,  $p_0 = -0.09 \pm 0.05$ ,  $p_1 = 0.044 \pm 0.021$ ,  $p_2 = -0.0051 \pm 0.0028$ ,  $p_3 = 0.00019 \pm 0.00012$

### 4.3 $K^-/K^+$ , $\pi^-/\pi^+$ and $p^-/p^+$ ratios

Figures 14 - 19 show the collision energy dependence of the particle ratios  $K^-/K^+$ ,  $\pi^-/\pi^+$  and  $p^-/p^+$  at different values of  $|\eta| < 0.1, 0.5$ , with respected fits of these dependencies.

Figures 14, 17 show that in  $K^-/K^+$  there is a sharp increase with increasing energy. This dependence corresponds to the results obtained in the experiment. The Figure 15, 18 shows that  $\pi^-/\pi^+$  is found to decrease with increase of  $\sqrt{s_{NN}}$ . Finally, the figures 16 and 19 show the dependence for the ratio  $p^-/p^+$ , but due to poor statistics for antiprotons and an excess of protons that did not participate in the interaction, the errors are too large for this data-set.

Figure 20 represent the ratio of charged particles  $\pi^-/\pi^+$ ,  $K^-/K^+$ ,  $p^-/p^+$   $K^+/\pi^+$  and  $K^-/\pi^-$  with pseudorapidity cut  $|\eta| < 0.1, 0.5$  and  $0.2 < p_T < 1.4$ . Uncertainties on experimental data represent statistical errors only. Here, the uncertainties are smaller than the symbol size.

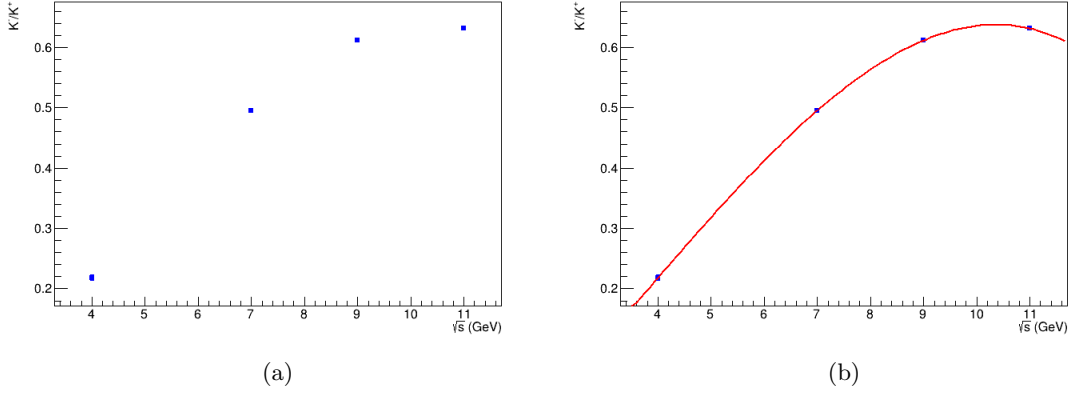


Figure 14: The ratio  $K^-/K^+$  for the four calculated energies  $\sqrt{s_{NN}} = 4, 7, 9, 11$  GeV with pseudorapidity cut  $|\eta| < 0.5$  and  $0.2 < p_T < 1.4$  (a) and fitted by polynomial function (b). The parameters of fit:  $\chi^2 = 1.51521e - 22$ ,  $p_0 = -0.16 \pm 0.07$ ,  $p_1 = 0.073 \pm 0.029$ ,  $p_2 = 0.008 \pm 0.004$ ,  $p_3 = 0.00075 \pm 0.00017$ .

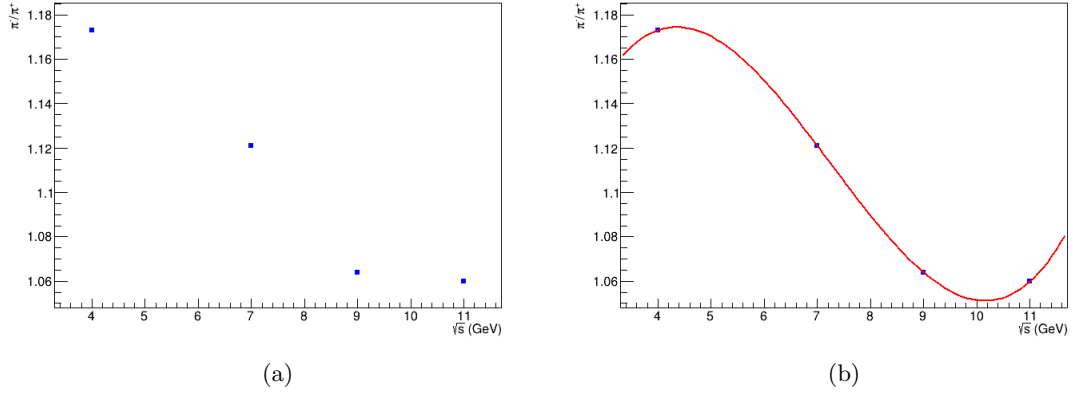


Figure 15: The ratio  $\pi^-/\pi^+$  for the four calculated energies  $\sqrt{s_{NN}} = 4, 7, 9, 11$  GeV with pseudorapidity cut  $|\eta| < 0.5$  and  $0.2 < p_T < 1.4$  (a) and fitted by polynomial function (b). The parameters of fit:  $\chi^2 = 9.24075e - 21$ ,  $p_0 = 0.861 \pm 0.013$ ,  $p_1 = 0.168 \pm 0.006$ ,  $p_2 = -0.0012 \pm 0.0008$ ,  $p_3 = 0.00127 \pm 0.00003$ .

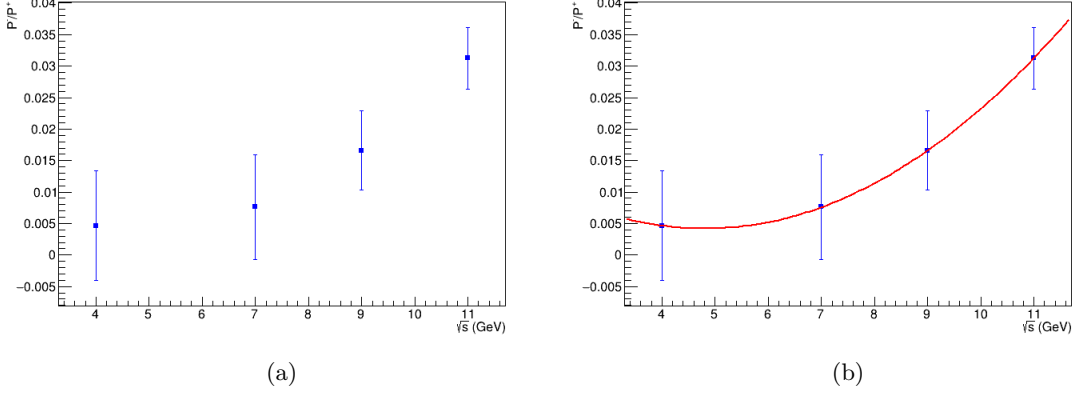


Figure 16: The ratio  $p^-/p^+$  for the four calculated energies  $\sqrt{s_{NN}} = 4, 7, 9, 11$  GeV with pseudorapidity cut  $|\eta| < 0.5$  and  $0.2 < p_T < 1.4$  (a) and fitted by polynomial function (b). The parameters of fit:  $\chi^2 = 7.62888e - 05$ ,  $p_0 = 0.021 \pm 0.004$ ,  $p_1 = -0.0068 \pm 0.0009$ ,  $p_2 = 0.0007 \pm 0.0006$ .

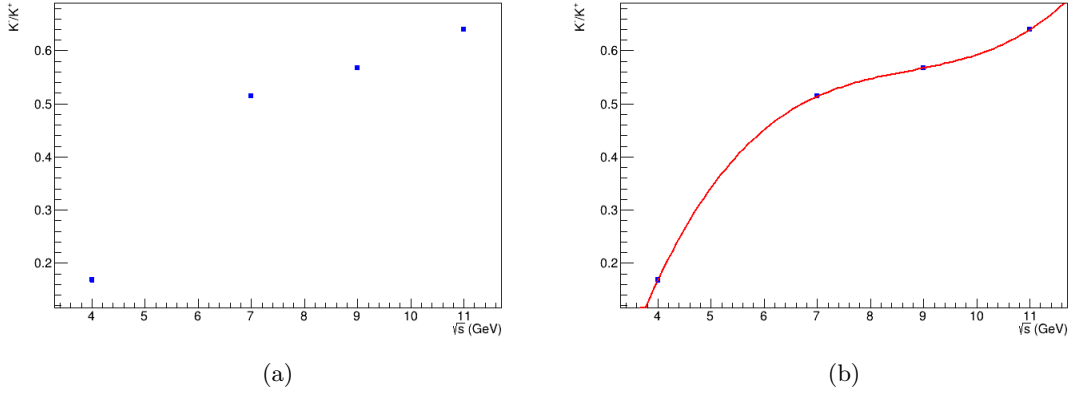


Figure 17: The ratio  $K^-/K^+$  for the four calculated energies  $\sqrt{s_{NN}} = 4, 7, 9, 11$  GeV with pseudorapidity cut  $|\eta| < 0.1$  and  $0.2 < p_T < 1.4$  (a) and fitted by polynomial function (b). The parameters of fit:  $\chi^2 = 1.4071e - 19$ ,  $p_0 = -1.51 \pm 0.07$ ,  $p_1 = 0.674 \pm 0.029$ ,  $p_2 = -0.075 \pm 0.004$ ,  $p_3 = 0.00286 \pm 0.00018$ .

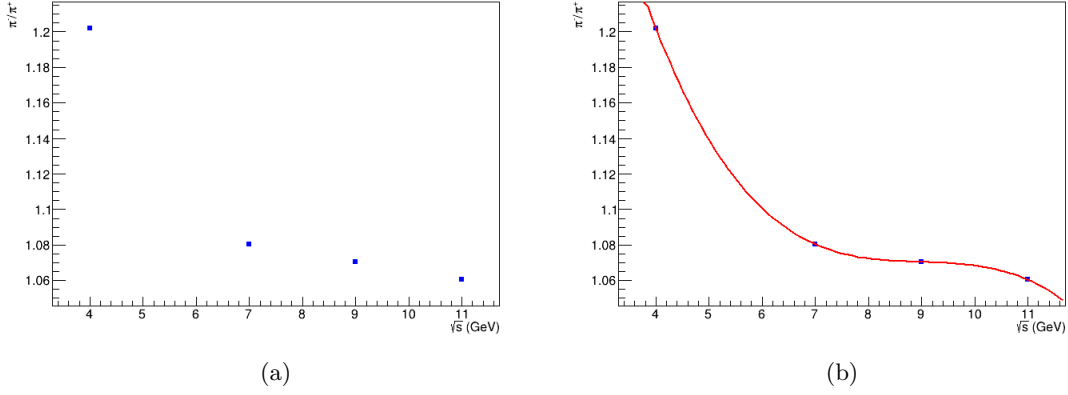


Figure 18: The ratio  $\pi^-/\pi^+$  for the four calculated energies  $\sqrt{s_{NN}} = 4, 7, 9, 11$  GeV with pseudorapidity cut  $|\eta| < 0.1$  and  $0.2 < p_T < 1.4$  (a) and fitted by polynomial function (b). The parameters of fit:  $\chi^2 = 9.29607e-22$ ,  $p_0 = 1.817 \pm 0.013$ ,  $p_1 = -0.247 \pm 0.006$ ,  $p_2 = 0.0273 \pm 0.0008$ ,  $p_3 = -0.00101 \pm 0.00003$ .

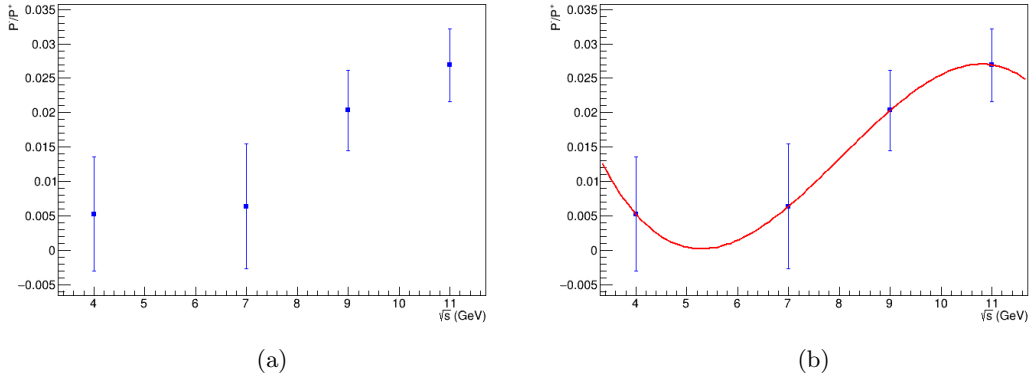


Figure 19: The ratio  $p^-/p^+$  for the four calculated energies  $\sqrt{s_{NN}} = 4, 7, 9, 11$  GeV with pseudorapidity cut  $|\eta| < 0.1$  and  $0.2 < p_T < 1.4$  (a) and fitted by polynomial function (b). The parameters of fit:  $\chi^2 = 2.23841e-22$ ,  $p_0 = 0.23 \pm 0.19$ ,  $p_1 = -0.054 \pm 0.008$ ,  $p_2 = 0.0077 \pm 0.0012$ ,  $p_3 = -0.00032 \pm 0.00005$ .

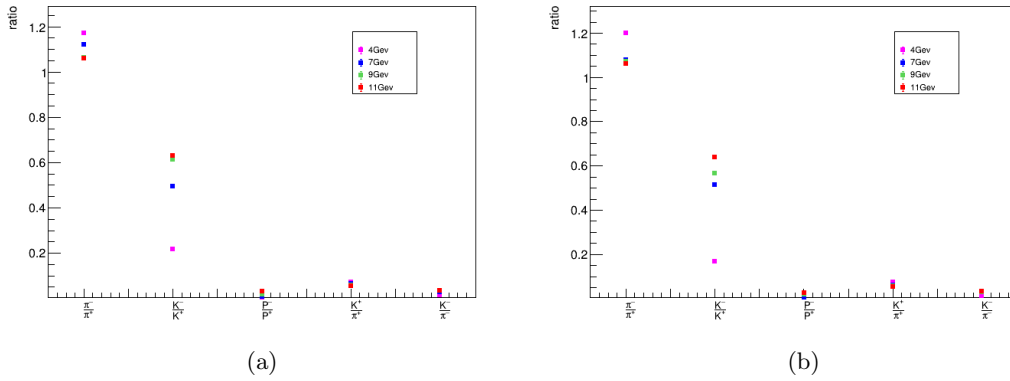


Figure 20: The ratio of charged particles  $\pi^-/\pi^+$ ,  $K^-/K^+$ ,  $p^-/p^+$ ,  $K^+/\pi^+$ ,  $K^-/\pi^-$  depending on the type of particles for different energies  $\sqrt{s_{NN}} = 4, 7, 9, 11$  GeV superimposed map by transverse momentum  $0.2 < p_T < 1.4$  and pseudorapidity (a)  $|\eta| < 0.5$ , (b)  $|\eta| < 0.1$ .

## 5 Conclusion

Collisions of heavy ions  $Au - Au$  in the energy range of the center of mass  $\sqrt{s_{NN}} = 4, 7, 9$  and  $11$  GeV were analyzed. The statistics of  $10^6$  events for each energy was obtained with the Monte-Carlo generator UrQMD. The simulation results were compared with experimental data. Histograms were made for transverse momentum  $p_T$  dependence of particle production for  $\pi^+$ ,  $\pi^-$ ,  $K^+$ ,  $K^-$ ,  $p^+$ ,  $p^-$  and depending on the relation in  $K^-/\pi^-$  and  $K^+/\pi^+$ , in  $K^-/K^+$ ,  $\pi^-/\pi^+$  and  $p^-/p^+$  for different collision energies. To make further and deeper analysis, it is necessary to analyze more statistics using different Monte-Carlo models for different values of the center-of-mass collision energy. In addition, different cuts can be applied, varying the conditions of the analyzed collisions. For  $K^-/K^+$  and  $\pi^-/\pi^+$  the dependence is in accordance with the experimental observations.

## 6 Acknowledgements

I would like to thank the Organizing Committee of the summer student program of the Joint institute for nuclear research for the amazing opportunity to be a part of this program. I would like to thank my supervisor Alexey Aparin for his support during my stay and for the opportunity to work at JINR. Finally, special thanks to my colleague Tatyana Nikolaeva for her support during the practice.

## References

- [1] B. Abelev et al., Systematic Measurements of Identified Particle Spectra in pp, d+Au and Au+Au Collisions from STAR, Phys. Rev., C79, 034909, (2009).
- [2] STAR Collaboration, "Studying the Phase Diagram of QCD Matter at RHIC", (2014). <https://drupal.star.bnl.gov/STAR/starnotes/public/sn0598>
- [3] C. Alt et al. (NA49 Collaboration), Phys. Rev. C 77, 024903 (2008).
- [4] <http://nica.jinr.ru/projects/mpd.php>
- [5] NICA White Paper: "Searching for a QCD mixed phase at the nucleon-based collider facility", v 10.01, (2014).
- [6] <http://mpd.jinr.ru/mpd/>
- [7] The NA49 Collaboration: S. V. Afanasiev, et al "Energy Dependence of Pion and Kaon Production in Central Pb+Pb Collisions", Phys. Rev. C66 054902, (2002).